Accident Analysis and Prevention 149 (2021) 105803

Contents lists available at ScienceDirect

Accident Analysis and Prevention

journal homepage: www.elsevier.com/locate/aap

The predictive capacity of the MADYMO ellipsoid pedestrian model for pedestrian ground contact kinematics and injury evaluation

Shi Shang [a], Catherine Masson [b], Maxime Llari [b], Max Py [b], Quentin Ferrand [b], Pierre-Jean Arnoux [b], Ciaran Simms [a,*]

[a] Trinity Centre for Bioengineering, Trinity College Dublin, Ireland
[b] Laboratoire de Biomécanique Appliquée (IFSTTAR – Université de la Méditerranée), France

ARTICLE INFO

Keywords:
Pedestrians
Vehicle contact
Ground contact
MADYMO model assessment

ABSTRACT

Pedestrian injuries occur in both the primary vehicle contact and the subsequent ground contact. Currently, no ground contact countermeasures have been implemented and no pedestrian model has been validated for ground contact, though this is needed for developing future ground contact injury countermeasures. In this paper, we assess the predictive capacity of the MADYMO ellipsoid pedestrian model in reconstructing six recent pedestrian cadaver ground contact experiments. Whole-body kinematics as well as vehicle and ground contact related a*HIC* (approximate *HIC*) and *BrIC* scores were evaluated. Reasonable results were generally achieved for the timings of the principal collision events, and for the overall ground contact mechanisms. However, the resulting head injury predictions based on the ground contact *HIC* and *BrIC* scores showed limited capacity of the model to replicate individual experiments. Sensitivity studies showed substantial influences of the vehicle-pedestrian contact characteristic and certain initial pedestrian joint angles on the subsequent ground contact kinematics and injury predictions. Further work is needed to improve the predictive capacity of the MADYMO pedestrian model for ground contact injury predictions.

1. Introduction

The World Health Organization (WHO) estimates that more than 300,000 pedestrians have died in 2019 (WHO, 2020), based on its Global Status Report on Road Safety 2018 (WHO, 2018). Pedestrian collisions usually involve a primary contact with the vehicle, followed by a secondary contact with the ground (Han et al., 2018; Shang, 2020). Accordingly, although most research has focused on vehicle contact (Kerrigan et al., 2007; Yao et al., 2008), the significance of the ground contact has also been emphasized (Simms and Wood, 2006; Crocetta et al., 2015; Han et al., 2018; Shang et al., 2018; Shi et al., 2019; Shang et al., 2020). A recent analysis based on German real-world crash data (GIDAS) showed that 43 % of 1221 selected cases had injuries subjected to ground contact, demonstrating the importance of ground related pedestrian injuries and providing significant motivation for countermeasures to prevent or moderate pedestrian injuries from ground contact (Shang et al., 2018). (Shang et al., 2020) recently conducted six cadaver tests which recorded the whole process from vehicle contact until after the end of the ground contact. They observed that peak linear accelerations in ground contact are generally higher than for the vehicle contact. They also observed a high predicted risk of rotationally induced brain injury from ground contact, even for very low vehicle collision speeds.

However, many open questions remain regarding the influence of vehicle front shape and the design of potential countermeasures to minimize pedestrian ground contact injuries, and a suitably validated computational model is a much more sustainable tool for addressing these than cadaver experiments.

The MADYMO 50th percentile male pedestrian model, developed by TNO Automotive, is the most commonly used multibody pedestrian model for vulnerable road user crash reconstruction (van Hoof et al., 2003; van Rooij et al., 2003; Simms and Wood, 2006; Untaroiu et al., 2009; Elliott et al., 2012; Xu et al., 2016; Shang et al., 2018). The model has been validated for both full body (Ishikawa et al., 1993) and segment level, such as tibia and femur static 3-point bending tests, cadaver side impact tests for the pelvis, thorax and shoulder, and cadaver leg impactor tests for bending moment and shear force evaluations (Kajzer et al., 1993). De Lange et al. (DeLange et al., 2006) verified the

* Corresponding author.
E-mail addresses: sshang@tcd.ie (S. Shang), csimms@tcd.ie (C. Simms).

https://doi.org/10.1016/j.aap.2020.105803
Received 22 June 2020; Received in revised form 28 August 2020; Accepted 22 September 2020
Available online 10 November 2020

kinematics of the MADYMO pedestrian model with eighteen full vehicle-pedestrian impact tests. However, the validation was only for vehicle contact and not for ground contact, even though it has since been applied for analyzing the ground contact (Crocetta et al., 2015; Zou et al., 2019). (Crocetta et al., 2015) defined six different pedestrian ground impact mechanisms by simulating hundreds of impact configurations with different vehicle shapes, pedestrian heights and vehicle speeds, with partial validation by comparison to real-world videos (Barry and Simms, 2016). The model has also been applied in the use of potential braking related countermeasures (Zou et al., 2019). However, the capacity of the MADYMO pedestrian model to replicate the kinematics of individual pedestrian ground contact collisions remains unknown.

Researchers have also developed other multibody or finite element pedestrian models for vehicle-pedestrian collisions. (Yang and Lovsund, 1997) developed a multibody pedestrian model with emphasis on the head and lower extremities. The model consists of fifteen body segments with fourteen joints. The leg segments are breakable (Yang et al., 1993) and the knee joint formulation (Yang et al., 1995) facilitates biofidelic responses of the knees and leg fracture. The model was validated based on pedestrian substitutes' kinematics, the body segments' accelerations, contact forces, and failure descriptions compared with previously published cadaver impacts (Ishikawa et al., 1993). Finite element pedestrian models such as THUMS (Maeno and Hasegawa, 2001; Iwamoto et al., 2003) and GHBMC (Untaroiu et al., 2016) pedestrian models are developed to simulate deformable vehicle-pedestrian impact scenarios. However, none of these models have been validated for ground contact.

In summary, a variety of pedestrian models (multibody and finite element) have been developed and applied to vulnerable road user crashes. These have been validated based on lower extremity bending and shear loadings, the head response including acceleration and force, head trajectories, whole-body kinematics etc. However, all models are validated for the vehicle impact only, and model validations for ground contact are so far lacking. The importance of pedestrian ground contact is growing and the risk of suffering serious head brain injury due to ground contact has been recently highlighted (Shang et al., 2018, 2020). Given the high cost of cadaver tests, there is significant value in a pedestrian model which can simulate the ground impact and can be applied in a large-sample parametric study (Li et al., 2018). The recent staged cadaver impact tests (Shang et al., 2020) provide a valuable experimental reference set, including pedestrian kinematics and injury criteria evaluations (skull fracture, *HIC* and *BrIC*) for multi-body model assessment.

Accordingly, the aims of the current study are to:

1) reconstruct the cadaver impact tests of (Shang et al., 2020) to assess the capability of the MADYMO pedestrian model for use in ground contact scenarios, and assess the difference between the MADYMO multibody model and the cadaver in post-impact kinematics and head injury criteria predictions.
2) Perform sensitivity studies to assess the influence of the vehicle pedestrian contact characteristics, the influence of initial pedestrian position on subsequent pedestrian ground contact and the effect of internal damping on overall body kinematics.

If the pedestrian model can reasonably replicate kinematics and injury outcomes, it may be suitable for investigating the effect of vehicle front shape on the risk of pedestrian ground contact injuries over a broad range of collision configurations. Moreover, it could be used for developing active countermeasures to prevent pedestrian ground contact related injuries, such as controlled braking or airbag technologies (Khaykin and Larner, 2016; Zou et al., 2019).

2. Materials and methods

The MADYMO ellipsoid multibody pedestrian model, as well as simplified vehicle models, were employed to assess their performance in ground contact, by comparison with the cadaver tests reported in (Shang et al., 2020), see Fig. 1.

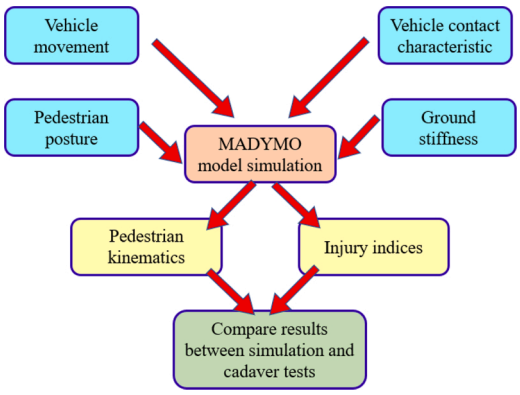

Fig. 1. Steps followed in assessing the multibody models.

Given uncertainty in several input characteristics of the models, sensitivity studies were designed to assess the influence of the vehicle/pedestrian contact definition (loading and unloading functions, hysteresis), internal damping in the pedestrian models and the initial pedestrian joint angles.

2.1. Multibody vehicle models

Simplified multibody vehicle models were built in MADYMO, with the geometry based on (The-Blueprints, 2020) to represent the vehicles tested in (Shang et al., 2020). Three different types of vehicle were chosen to represent a wide range of bonnet leading edge height (BLEH). Each vehicle model consists of a lower bumper, bumper, bonnet leading edge, bonnet, windshield, wheels and roof, see Fig. 2.

2.2. Pedestrian models

The heights and weights of the pedestrian cadavers varied, as shown in Table 1 of (Shang et al., 2020), replicated here as Appendix A and these were replicated by scaling the MADYMO 50th percentile pedestrian model using a customized Matlab code based on the pedestrian's height and weight. This global scaling does not address relative differences in body segment proportions. The scaled multibody models, as well as the corresponding pedestrian cadavers in side views and front views are shown in Fig. 3. The initial postures (joint angles) of the models were adjusted based on the measurements of cadaver poses from the side and the front views which were captured pre-impact. Due to the joint definitions in the pedestrian model and body segment dimension differences, some differences between cadaver and the simulation postures exist, see for example the left forearm in Fig. 3(a). For Test 05 in Fig. 3(e), the posture is the result of difficulties with initial placement of the cadaver which had very low mass (38 kg) and unusually stiff joints (the cause of this is unknown as full medical histories were not available).

2.3. Movement input of the multibody vehicle models

The planar time-displacement curves in the X (horizontal) direction and the Z (vertical) direction, and the time-rotation curve of the vehicle, were extracted every 20 ms (overall impact duration was approximately one second) using a customized Matlab script and used to prescribe the vehicle motion in the models. The general steps for selecting the tracking points are as shown in Appendix B.

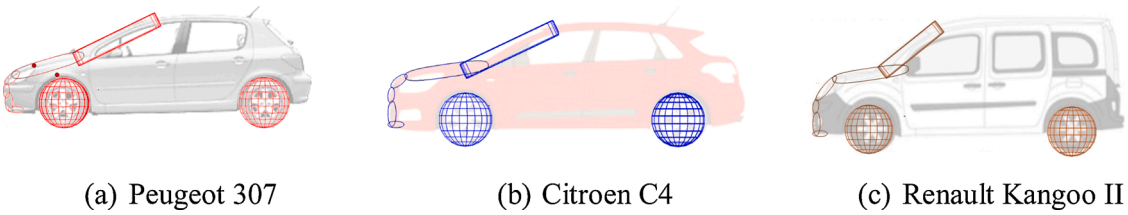

Fig. 2. The vehicle models with the simplified MADYMO models.

Table 1
The input parameter of the multibody sphere (simplified head model).

Parameter	Input
Head Mass	4.5kg
Inertia	(2.08e-02 2.37e-02 1.53e-02 0 0 0) kg·m^2 (directly from MADYMO 50th percentile pedestrian model)
Linear speed	From (Shang et al., 2020)
Angular speed	From (Shang et al., 2020)
Initial position	0.02 m high from the ground in vertical direction

2.4. Contact characteristic applied on the MB vehicle model

Three sources of vehicle contact characteristic were available: the published force-deformation characteristics derived from impactor tests (Martinez et al., 2007), recent tests on the actual vehicle types performed by the European New Car Assessment Programme (Euro-Ncap, 2020) (Euro-Ncap, 2020) and another older force deformation characteristics from published impactor tests (Mizuno and Kajzer, 2000) and (Liu et al., 2002). The windshield and bonnet stiffness from (Mizuno and Kajzer, 2000) were obtained by impactor tests and the stiffness of the bonnet leading edge and bumper were obtained from legform tests by (Liu et al., 2002). This combination of vehicle contact characteristic has previously been used by (Li et al., 2016) for a virtual test system. Euro NCAP assesses the pedestrian safety performance of new cars with a rating (up to 5-star) based on sub-system impactor tests (Hobbs and McDonough, 1998; Euro-NCAP, 2010). (Martinez et al., 2007) summarized 425 Euro NCAP tests and then estimated a series of simplified average stiffness curves. The force-deformation curves of each tested vehicle from the Euro NCAP tests as well as the force-deformation curves from (Martinez et al., 2007) and (Mizuno and Kajzer, 2000) are shown in Fig. 4. The detailed process of obtaining the vehicle front stiffness by using subsystem impactors can be found in (Martinez et al., 2007).

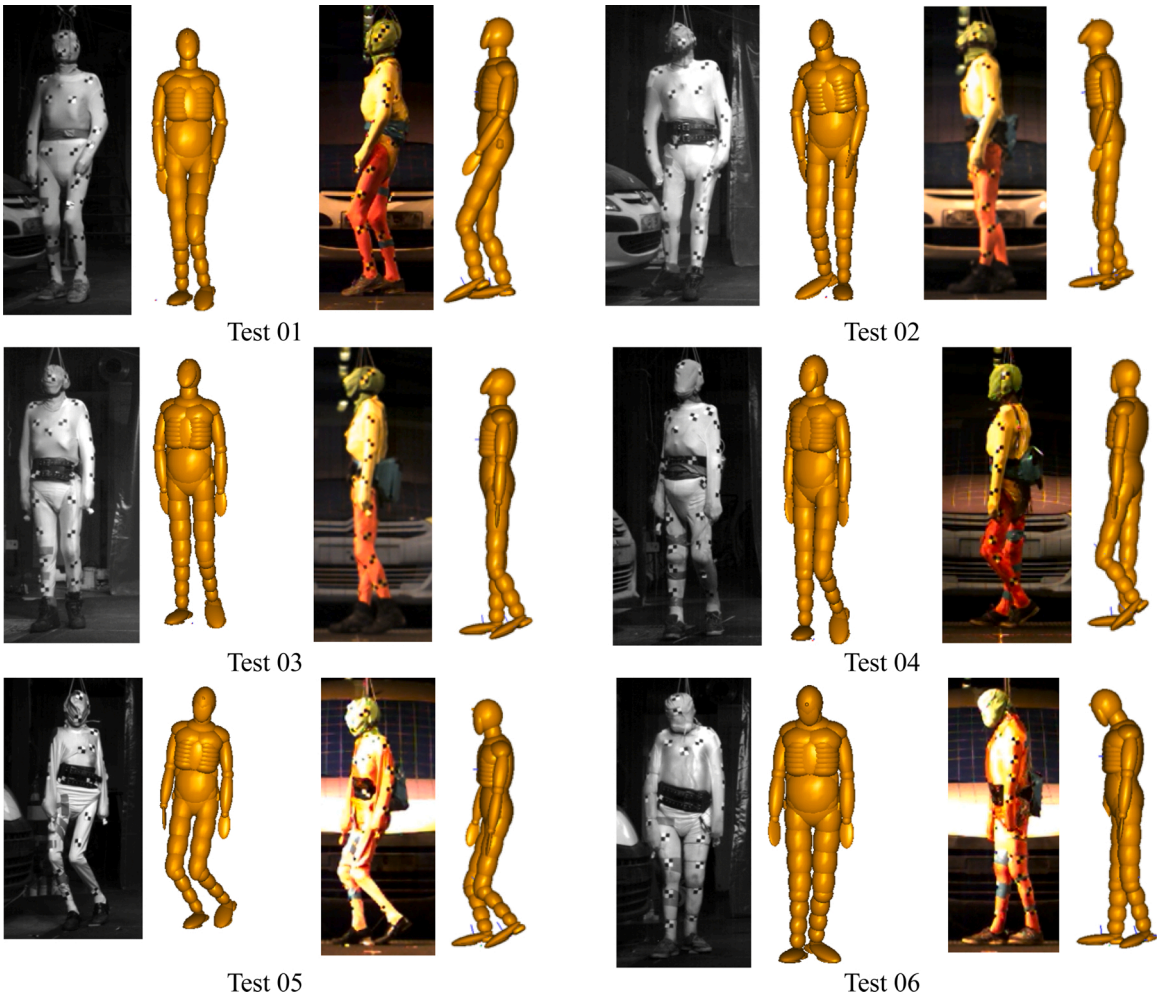

Fig. 3. The initial postures of PMHS pedestrians and the corresponding scaled multi-body models.

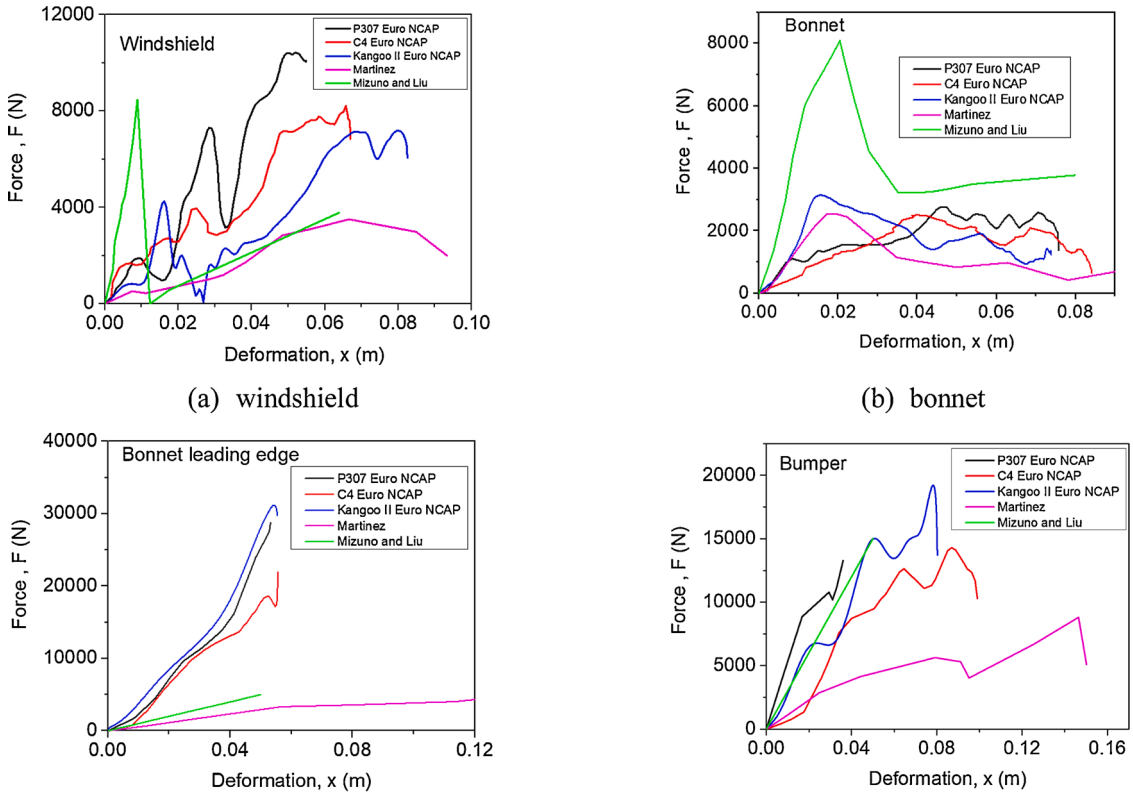

Fig. 4. Force-deformation contact characteristics of vehicle front components from different sources.

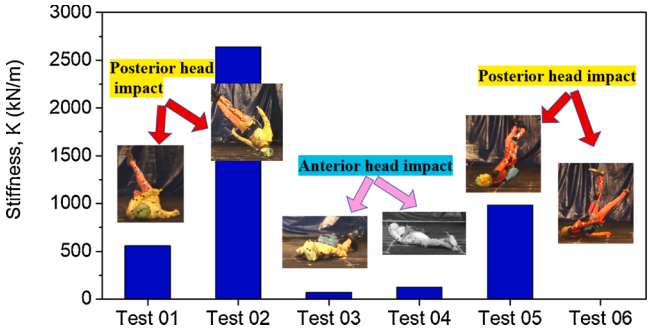

Fig. 5. Ground stiffness for each test calculated.

2.5. Ground contact stiffness

Considering the individual differences between the tested cadavers and also the different locations on the head (some of the head contacts occurred to the face while others occurred to the posterior of the head), the ground contact stiffness was set individually in MADYMO for each reconstruction. To estimate the contact stiffness, a multibody sphere with inertia properties matching the head and initial linear and angular velocities matching the experimental head kinematics just prior to head ground contact was used to simulate the head impacts with the ground, see Table 1. The method used to estimate the contact stiffness of the ground was based on the assumption that a quarter wave of simple harmonic motion (Triana and Fajardo, 2013) reasonably models head acceleration until the peak is reached in the head ground impact, see Eq. 1. From this, stiffness is calculated based on the peak acceleration and speed change.

$$\sqrt{\frac{m}{K}} = \omega = \frac{1}{\Delta T} = \frac{1}{\left(\frac{\Delta V}{Acc_{peak}}\right)} = \frac{Acc_{peak}}{\Delta V}$$
$$K = m \times \left(\frac{\Delta V}{Acc_{peak}}\right)^2 \quad (1)$$

where m is the mass of the head, ω is the natural frequency, ΔT is the time duration of the impact, ΔV is the speed change during impact and Acc_{peak} is the peak acceleration. The stiffness (K) calculated for each test and the anterior/posterior head contact location are shown in Fig. 5. The head ground contact characteristics for Test 06 is not listed as the acceleration measurement was corrupted during ground contact. As the input of Test 06 was similar to Test 05 and the pedestrian ground contact mechanisms of the two tests were same, the stiffness of the ground for Test 06 was set as same as that of Test 05. The comparison of the accelerations obtained from the simplified head model with the corresponding cadaver tests are illustrated in Fig. 6, and the average values were applied for posterior and anterior head contacts. The average value of K from Test 01, Test 02 and Test 05 was used to define K_p (posterior), as shown in Table 2, for the 30 kph tests, which have a relatively high ground stiffness due to the posterior head impact. In contrast, in Test 03 and Test 04, the front softer part of the head, such as the nose and face impacted the ground first, namely the anterior head impact, and the ground contact stiffness in these two tests was set as K_a (anterior) as shown in Table 2, using the average value of K from the corresponding tests. K_p and K_a were then chosen as head ground contact characteristic depending on which area of the head impacts the ground first, as determined in a pre-simulation.

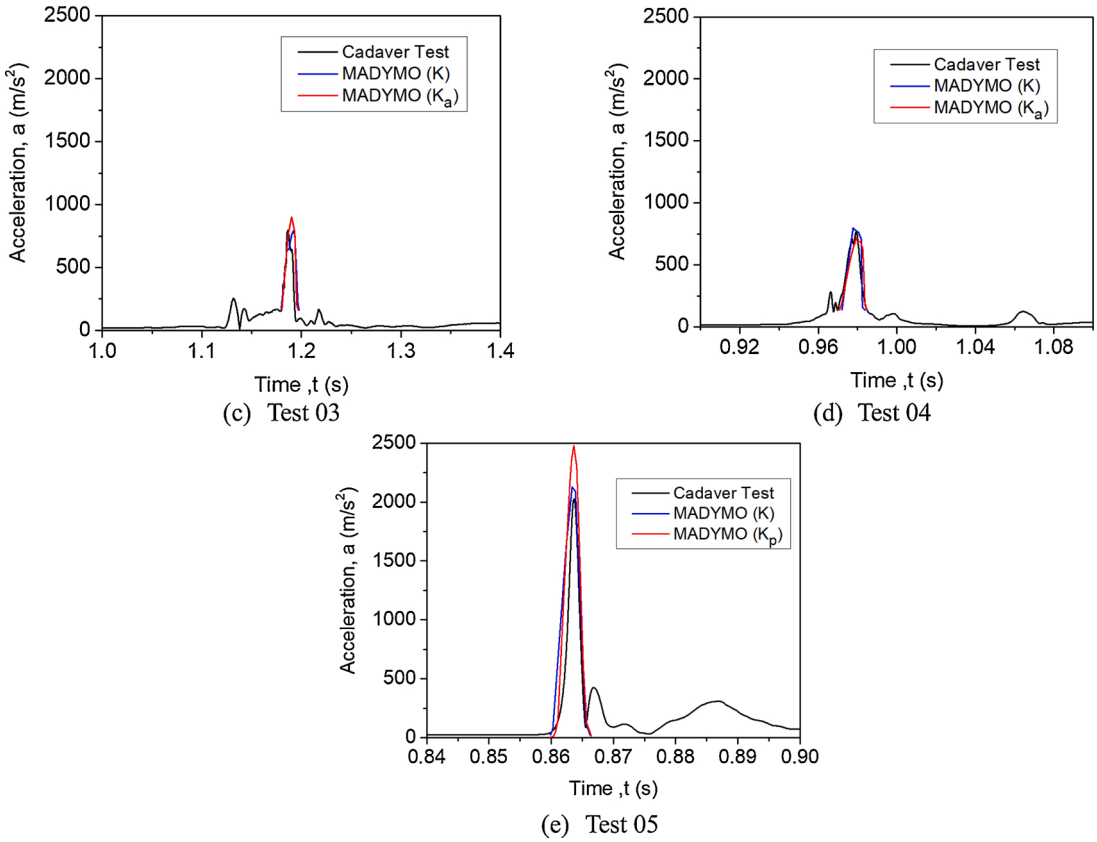

Fig. 6. Comparison of the accelerations obtained from simplified head model test by using K_a or K_p (the comparison of Test 06 was not given because the experimental head acceleration was corrupted).

Table 2
Stiffness of ground applied in MADYMO simulations.

	Value	Test used for reconstruction
k_p	1400 kN/m	Test 01, Test 02, Test 05 and Test 06
k_a	97 kN/m	Test 03 and Test 04

2.6. Injury assessment

Assessments of head injury caused by translational accelerations were approximated using the *HIC* criterion, whereas injuries caused by rotational angular velocities were approximated using the *BrIC* criterion. It is noted this is not the actual *HIC* as it was not possible to fix the accelerometer to head CG in the cadaver tests for practical reasons, while the accelerometers can be fixed in the mouth, it is possible to apply the *HIC* computation to the head accelerometer data with an approximate 10 % difference (Shang et al., 2020). Evaluation of *UBrIC* (Gabler et al., 2018) instead of *BrIC* (Takhounts et al., 2013) would be preferable but was not possible due experimental limitations in the cadaver tests of (Shang et al., 2020).

3. Simulation results

The six staged tests (Shang et al., 2020) were reconstructed and simulated using the MADYMO platform. Each test was simulated using the three different vehicle contact characteristics (Euro-Ncap, 2020), (Mizuno and Kajzer, 2000; Liu et al., 2002) and (Martinez et al., 2007), see Fig. 4. Pedestrian kinematics and head injury predictions (HIC and BrIC) from vehicle contact and ground contact were compared between the simulation and the corresponding experiment, see Fig. 7(and Fig. C1 in Appendix C for front view) and Fig. 8.

3.1. Pedestrian kinematics

The key event timings of the vehicle-pedestrian impact from the staged tests and simulations as well as the ground contact mechanisms are compared, see Table 3. The ground contact mechanisms are summarized by assessing the whole-body rotation angles and the posture before landing, with reference to the definition of (Crocetta et al., 2015). Overlaying the video still shots from the experiments with the simulations was not practical due to camera projection issues. In Test 01 and Test 02, pedestrian vehicle separation times are generally earlier in the simulations than in the cadaver tests. However, the head ground contacts occurred more than 100 ms earlier for the simulation in Test 01 but late in Test 02.

3.2. Pedestrian planar head trajectories

Pedestrian planar head trajectories (tracked based on the marker on the pedestrian's forehead) in both the X (horizontal, positive direction of vehicle travel) and Z (vertically upwards) directions from staged tests and the simulations are compared, see Fig. 8. Appendix Fig. B1 shows the definition of the coordinate system after (Shang et al., 2020). For Test 01 and Test 02, the horizontal head motion in the simulations is greater than was observed in the experiments.

3.3. Pedestrian head injury criteria assessments

The a*HIC* (approximate *HIC* as clarified in section 2.6) and *BrIC* scores were calculated for both vehicle and ground contact for all six cases and compared with the staged PMHS test results, as shown in Fig. 9. The average errors for the injury indices for both vehicle and ground contact over all six tests obtained from simulations using vehicle contact characteristics from Mizuno and Liu, Martinez and EU NCAP

Fig. 7. Sequences of vehicle-pedestrian impact experiment compared with MB simulations. Contact characteristic of vehicle front applied from (Green model: EU NCAP; Blue model: Martinez; Red model: Mizuno). (a) Test 01; (b) Test 02; (c) Test 03; (d) Test 04; (e) Test 05; (f) Test 05.

Fig. 7. (*continued*).

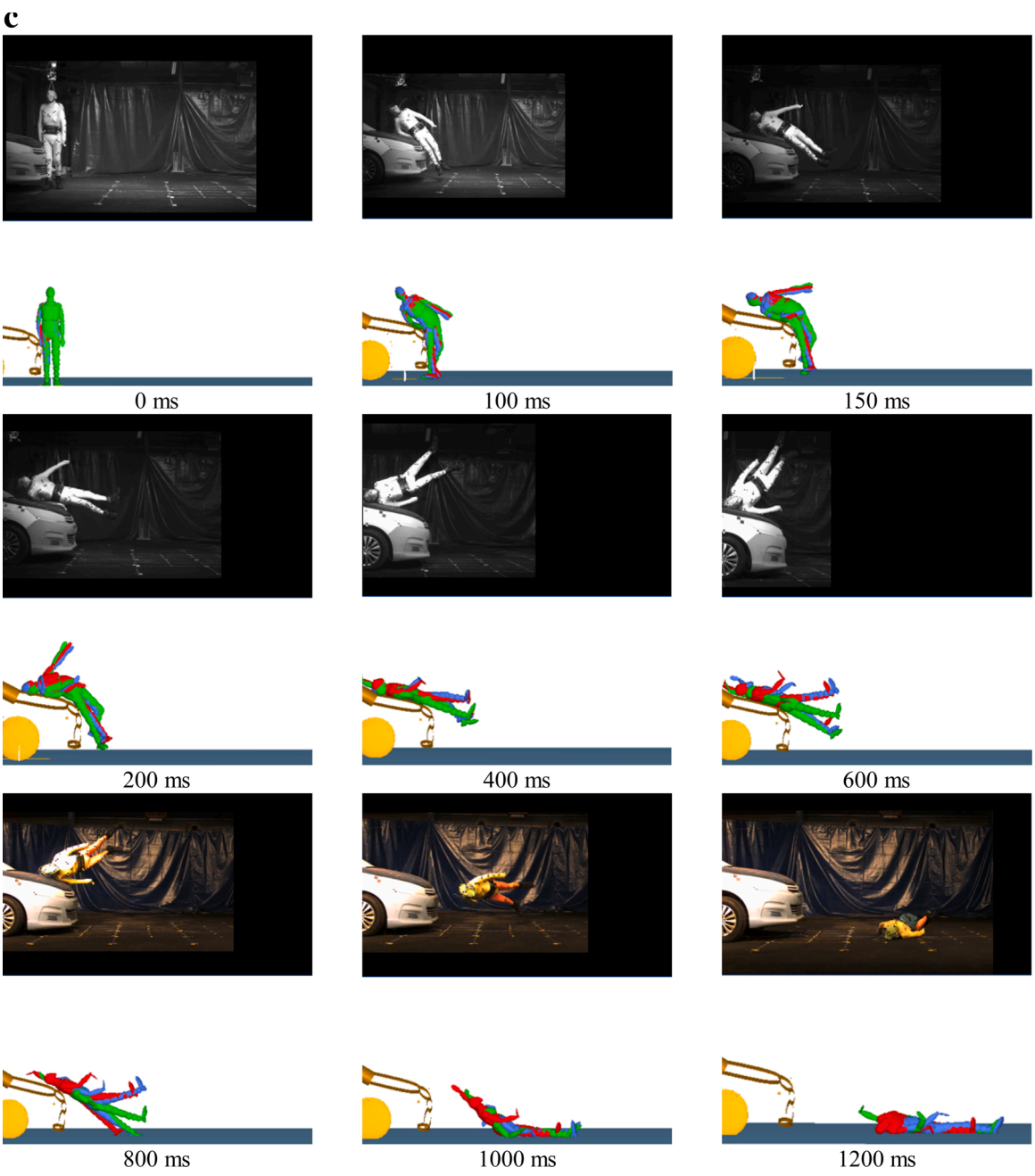

Fig. 7. (*continued*).

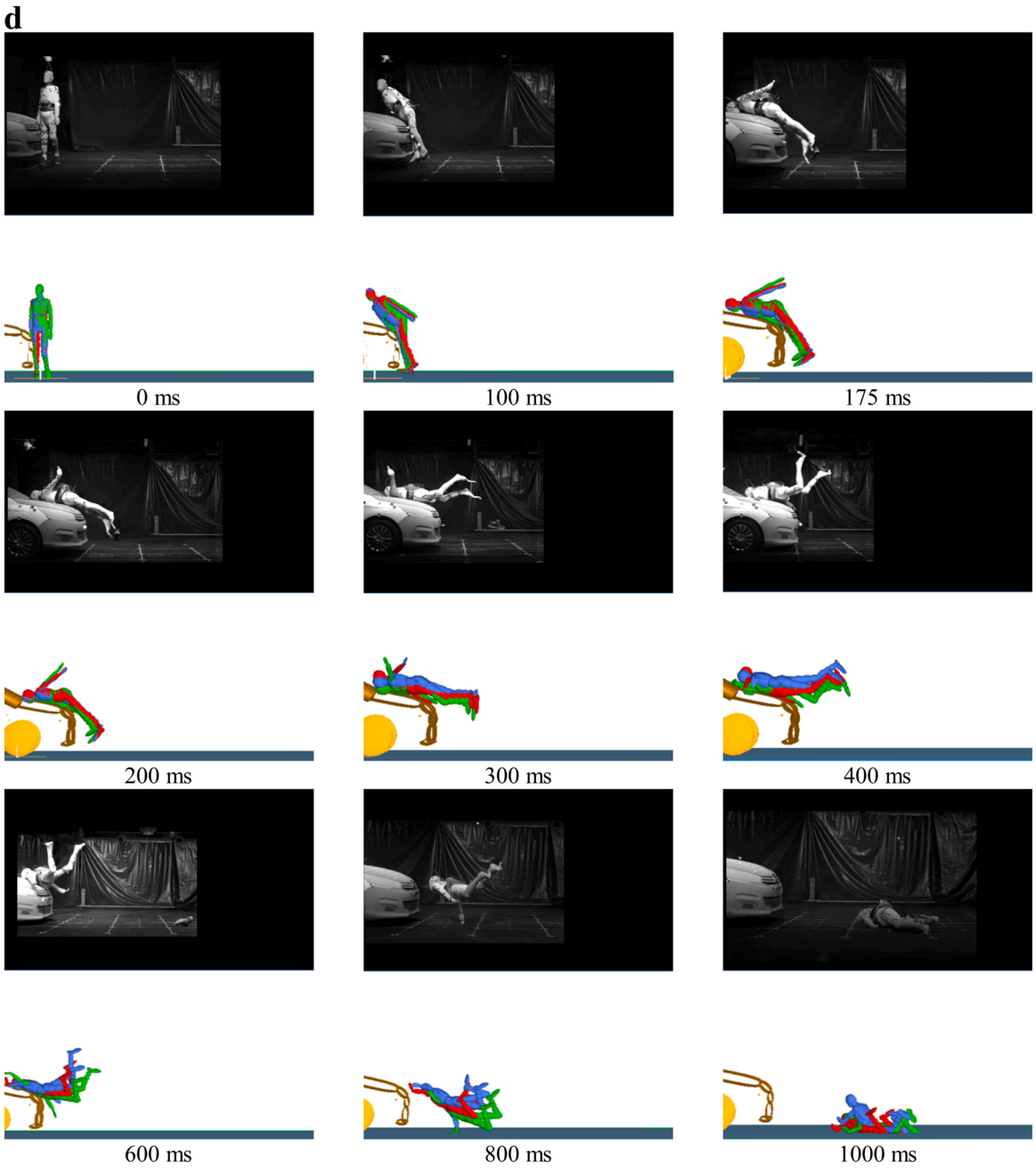

Fig. 7. (*continued*).

Fig. 7. (*continued*).

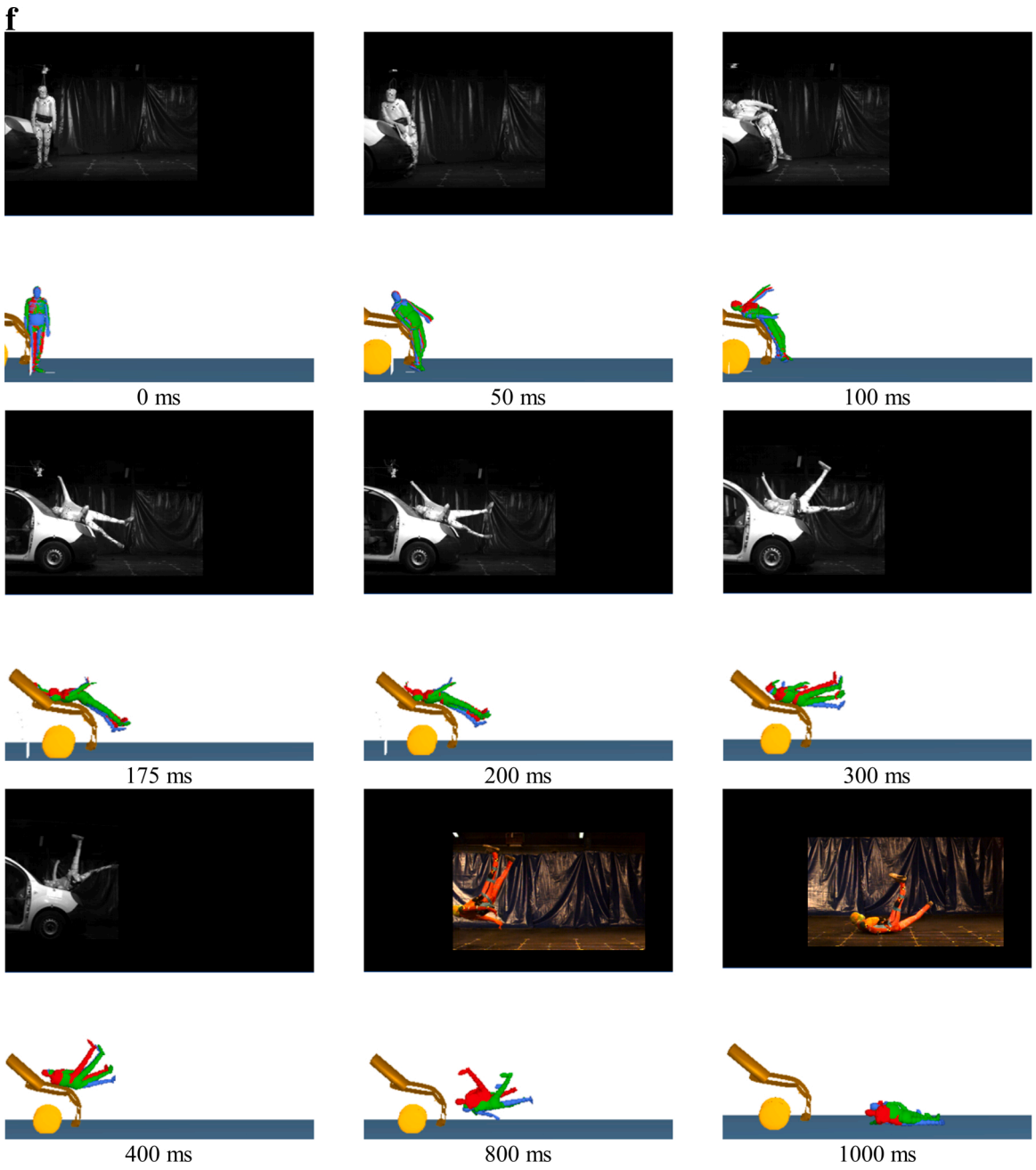

Fig. 7. (*continued*).

compared with the cadaver tests are 51.3 %, 62.0 %, 73.3 %, respectively.

4. Sensitivity study

The vehicle contact characteristics do not obviously affect the kinematics during the vehicle contact. However, Section 3.3 shows they do have a large influence on the secondary ground contact kinematics and the resulting injury predictions. The influence of the pedestrian initial joint angles and internal damping of the MADYMO pedestrian model are also of interest. In these sensitivity studies, the Mizuno and Liu's stiffness was used as the baseline for comparisons as this stiffness gave the smallest overall error, see Fig. 9.

4.1. Sensitivity study of hysteresis and unloading curve

Apart from the loading function, the hysteresis slope and unloading curve definitions in MADYMO further influence the contact modelling. The effects were tested based on the simplified head model impact simulations. The hysteresis slope over 5 magnitudes (9e4, 9e5, 9e6, 9e7 and 9e8, baseline value is 9e6) and the unloading curves in 3 different ratios (0%, 5% and 10 %, baseline value is 0%) of loading curve were tested, see Fig. 10. Results showed that lower hysteresis slopes produced relatively higher acceleration peaks and wider acceleration pulses which can greatly impact *HIC* scores. Altering the unloading curve showed a negligible effect on the peak and impact time duration.

4.2. Sensitivity study of pedestrian initial joint angle

The initial joint postures of the MADYMO pedestrian model were set

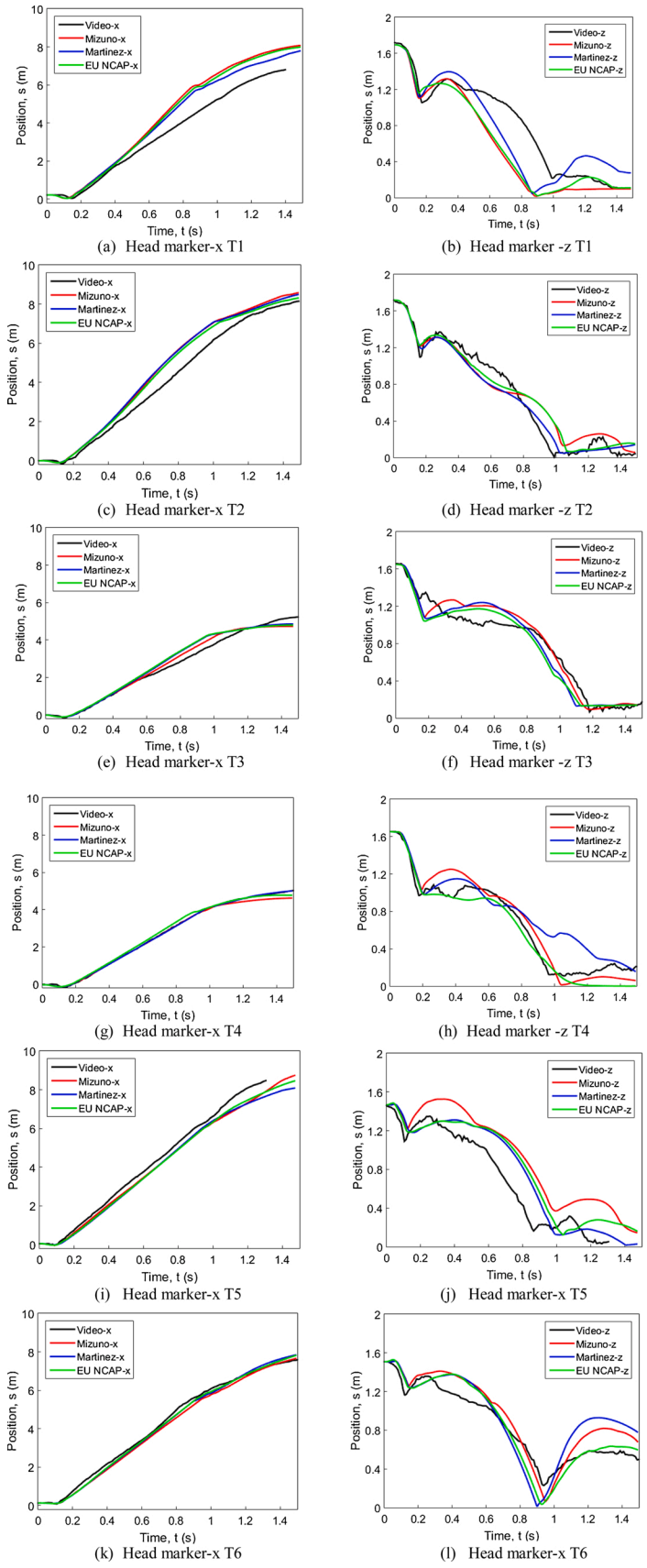

Fig. 8. Comparison of pedestrian forehead trajectories between cadaver experiments and simulations.

Table 3
Comparison of key events (s) of Test 01.

Contact characteristic source	$t_{head\text{-}vehicle\ contact}$ (s)	$t_{separation}$ (s)	$t_{head\text{-}ground\ contact}$ (s)	Ground contact mechanism, from (Crocetta et al., 2015)
Staged test	0.145	0.770	0.995	M1
Mizuno and Liu[a]	0.140	0.595	0.845	M3
Martinez	0.140	0.615	0.875	M3
EU NCAP	0.145	0.610	0.865	M3
Contact characteristic source	$t_{head\text{-}vehicle\ contact}$ (s)	$t_{separation}$ (s)	$t_{head\text{-}ground\ contact}$ (s)	Ground contact mechanism, from (Crocetta et al., 2015)
Staged test	0.153	0.710	0.986	M3
Mizuno and Liu	0.150	0.625	1.045	M3
Martinez	0.150	0.615	1.020	M3
EU NCAP	0.150	0.655	1.070	M3
Contact characteristic source	$t_{head\text{-}vehicle\ contact}$ (s)	$t_{separation}$ (s)	$t_{head\text{-}ground\ contact}$ (s)	Ground contact mechanism, from (Crocetta et al., 2015)
Staged test	No show	0.834	1.180	M2
Mizuno and Liu	0.170	0.845	1.1170	M2
Martinez	0.170	0.805	1.1095	M2
EU NCAP	0.160	0.800	1.1130	M2
Contact characteristic source	$t_{head\text{-}vehicle\ contact}$ (s)	$t_{separation}$ (s)	$t_{head\text{-}ground\ contact}$ (s)	Ground contact mechanism, from (Crocetta et al., 2015)
Staged test	0.169	0.740	0.970	M2
Mizuno and Liu	0.185	0.745	1.030	M2
Martinez	0.185	0.745	1.255	M2
EU NCAP	0.185	0.705	1.190	M2
Contact characteristic source	$t_{head\text{-}vehicle\ contact}$ (s)	$t_{separation}$ (s)	$t_{head\text{-}ground\ contact}$ (s)	Ground contact mechanism, from (Crocetta et al., 2015)
Staged test	0.098	0.647	0.860	M1
Mizuno and Liu	0.120	0.735	1.790[b]	M1/ M2
Martinez	0.120	0.735	0.990	M1/ M2
EU NCAP	0.115	0.735	1.040	M1/ M2
Contact characteristic source	$t_{head\text{-}vehicle\ contact}$ (s)	$t_{separation}$ (s)	$t_{head\text{-}ground\ contact}$ (s)	Ground contact mechanism, from (Crocetta et al., 2015)
Staged test	0.110	0.727	0.936	M1
Mizuno and Liu	0.135	0.725	0.945	M1/ M2
Martinez	0.135	0.690	0.895	M1/ M2
EU NCAP	0.130	0.680	0.925	M1/ M2

[a] The contact characteristics used in the simulations are from these authors correspondingly.
[b] The arm initially prevented the head from impacting the ground.

based on the measurement of the joint angles of captured images in different views of the cadavers just before testing (Shang et al., 2020). The effect of the joint angles was studied to assess the influence of joint angle on the resulting kinematics. Considering Test 01, the initial hip angle, knee angle and ankle angle of the struck leg were changed ± 5 degrees in YZ plane (see Table 4) to check the influence on the ground related head injury indices. Only one parameter was changed each time and the other two were kept constant (baseline) for this sensitivity study. The results are shown in Fig. 11. The injury indices obtained from the baseline model and the pedestrian with initial joint angle 2 (as illustrated in Table 4) are close, while for the pedestrian with initial hip joint angle 2 and knee joint angle 2, the injuries showed noticeable differences when compared with the baseline results, as did the ground contact mechanisms, see Fig. 12.

4.3. Sensitivity study of bending of pedestrian model

As seen in Test 01 and Test 02 shown in Fig. 7, the pedestrian model rebounced off the vehicle after the head windscreen impact, but this did not occur in the cadaver tests. Given the high levels of energy absorption in the contact definitions, a potential alternative reason for this could be insufficient internal damping in the pedestrian models. A sensitivity study of human model bending was therefore performed, with a modified damping coefficient of 100 N·s/m used to reconstruct Test 01 and compared with the baseline simulation (default damping values of MADYMO pedestrian model), see Fig. 13. The damping added to the model did not significantly reduce the rebound but did significantly change the post-impact kinematics and the mechanism of ground contact.

5. Discussion

Comparison of the predictive capacity of the MADYMO pedestrian model for injuries in the vehicle contact phase compared to the ground contact phase shows relatively high errors in both (Fig. 9). As vehicle contact has been previously validated (Coley et al., 2001; Serre et al., 2006) while there has been no previous attempt at validating the pedestrian model for ground contact, our emphasis here is on ground contact. This paper presents the first kinematics assessment of a multi-body pedestrian impact model for the phases following vehicle impact up to and including the ground contact, using cadaver test data for head kinematics and injury prediction comparisons.

Firstly, by comparing the cadaver impact tests with real-world crash videos which were analysed in Chapter 5 and Chapter 6 of (Shang, 2020), some differences can be observed. Around half of the pedestrians showed voluntary motions in the selected real-world videos while this obviously cannot occur in the cadaver tests. The voluntary motions may affect pedestrian post-impact kinematics and thus result in variable ground contact mechanisms. The cadavers rotated less than 270 degrees before landing in all the 6 tests, while for the videos with estimated vehicle speed between 20–30 kph, pedestrian whole body rotation angles vary from 90 degrees to 450 degrees. The reasons for this difference are not clear.

A computational model for assessing pedestrian ground contact injuries, and for possible use in the development of ground contact injury prevention countermeasures, has a number of hierarchical

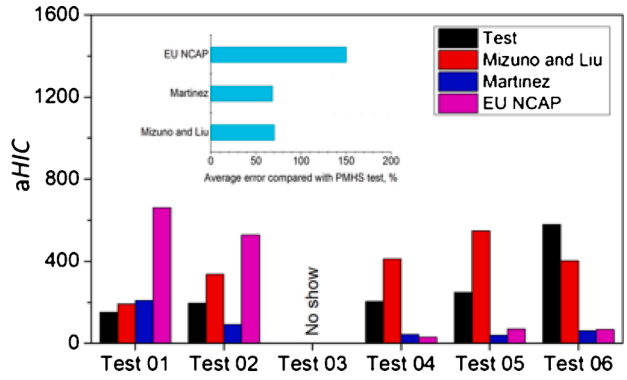

(a) *HIC* from vehicle contact

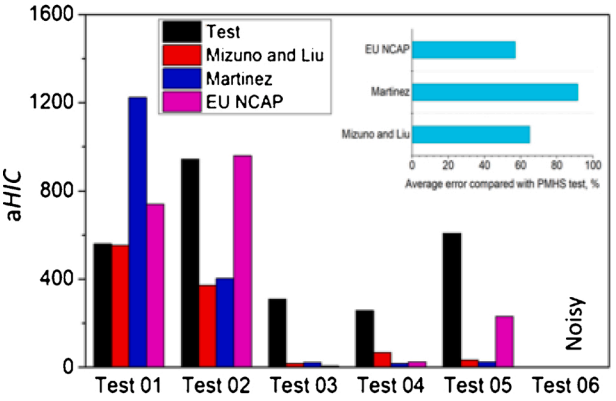

(b) *HIC* from ground contact

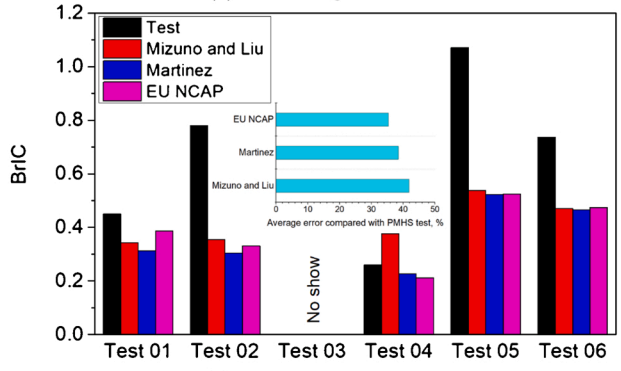

(c) *BrIC* from vehicle contact

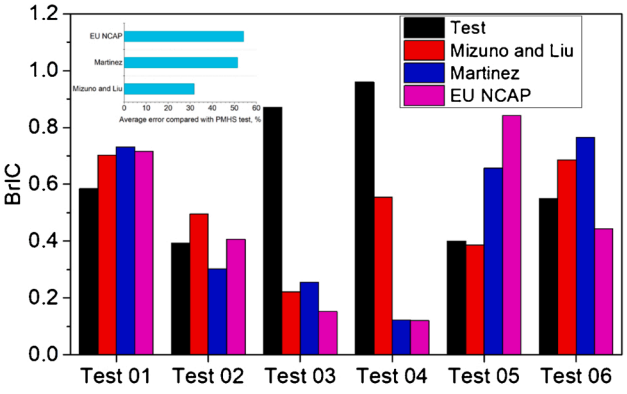

(d) *BrIC* from ground contact

Fig. 9. Comparison of head injury indices from vehicle and ground contact.

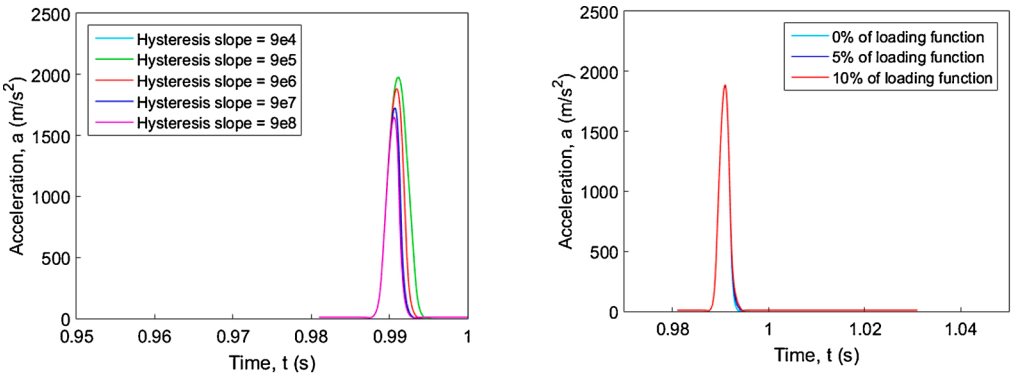

(a) Hysteresis slope (b) Unloading curve (hysteresis slope = 9e6)

Fig. 10. Testing of hysteresis slope and unloading curve effect on the contact using a simplified sphere model.

requirements. In terms of whole-body kinematics, there is the need for replicating the main body segment trajectories following the initial vehicle contact, followed by the pre-impact pose and velocity for the ground contact, especially the head. Subsequently, replicating the 6 DOF motion of the head and other body segments during ground contact is needed for injury criteria evaluation. For finite element models, tissue level stress/strain responses can be assessed, but this is beyond the scope of the current paper which focuses on the evaluation of the multibody MADYMO ellipsoid pedestrian model.

Table 4
Initial angles of joint sensitivity study.

Joint	Angle 1 (-5°)	Baseline angle (°)	Angle 2 (+5°)
Ankle	2 21	7 26	12 31
Knee	−5	0	5
Hip			

Table 3 shows that the timings of the head to vehicle contact are well reproduced for Test 01 and Test 02 of Shang et al., 2020, where the collision speed is 30 kph and the bonnet leading-edge height is 70 % of the hip height. However, for the 20kph cases (Tests 03 and 04) and the two high bonnet cases at 30 kph (Tests 05 and 06), there are substantial differences (of the order of 20 ms) in the head to vehicle contact times. For Tests 01 and 02 the models separate from the vehicle too early, suggesting insufficient energy absorption. However neither varying the contact characteristics nor introducing additional damping was successful in addressing this, and this is the focus of future work. The timing of the subsequent ground contact is poor in some cases (maximum error is 0.9 s in Test 05, see Table 3, where the arm of the pedestrian model prevented the head impacting the ground) but the correspondence to the pedestrian ground contact mechanisms identified by (Crocetta et al., 2015) is reasonable (correct mechanism identified in three cases, incorrect in one case, and partially correct in two cases. However, Fig. 7 shows some substantial differences in the flight trajectory and ground contact sequences. In consequence it is not surprising that the resulting injury criteria assessments in Fig. 9 show cases where very substantial differences between the model and the corresponding experiment are evident. Thus the current MADYMO pedestrian models cannot reliably distinguish the influence of the various factors varying between the different tests (vehicle shape and speed, body size and pose, vehicle contact characteristic). Previous validation of the MADYMO pedestrian model has focused on vehicle related kinematics and injuries at 40 kph (Coley et al., 2001; Serre et al., 2006). It is possible that some of the differences between the model and the experiment in the vehicle contact phase results from previous optimization of the model to replicate a 40 kph response. Regardless, the chain of events is such that failure to replicate the vehicle contact precludes a reasonable ground contact prediction.

The sensitivity studies show that the choice of vehicle contact characteristic makes a significant difference to pedestrian ground contact kinematics and injury evaluations, as do the hysteresis slope and the initial knee and hip angles. Somewhat surprisingly, the contact characteristic using the older data from impactor tests by Mizuno and Liu generally yielded the lowest errors for *HIC* in the vehicle contact (Fig. 9a), but the reliability of the resulting ground contact *HIC* is poor (Fig. 9b). Similarly, the predictions of the *BrIC* in both the vehicle and ground contacts are a poor match to the experimental data. However, the comparisons of the injury predictions indicated that the injuries from ground contact can be more severe than that from vehicle contact.

Increasing the internal damping in the pedestrian model does substantially affect the kinematics but did not improve the comparison with the experimental data. A further round of simulations was conducted with the goal of improving the match between the predicted and test ground impact mechanisms by changing the vehicle contact stiffness. The results are not presented here, but the outcome was that while this approach was successful in improving the ground contact kinematics, the resulting vehicle contact injury predictions were very different to the experiments.

A multi-body modelling environment such as MADYMO with a different pedestrian model implementation could in principle be used to

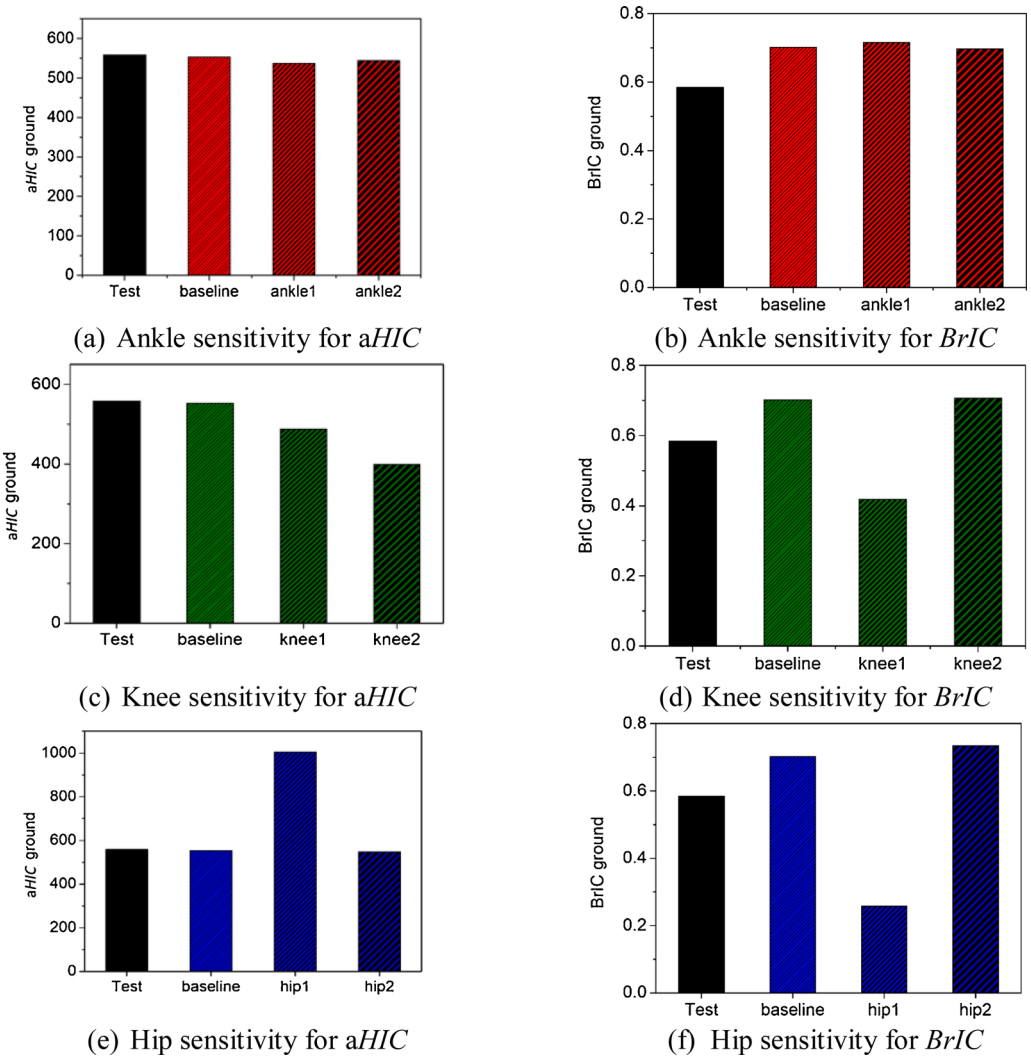

Fig. 11. Initial joint angle effect on a*HIC* and *BrIC* from ground contact for Test 01.

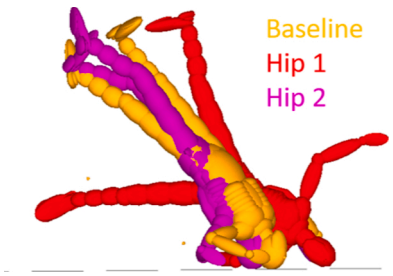

Fig. 12. Pedestrian ground contact mechanisms in Test 01 from different initial hip angle from Table 4.

effectively reconstruct the cadaver ground contact experiments we have performed. However, the purpose of this paper was specifically to assess the well-known and much used MADYMO ellipsoid pedestrian model. While the average errors for the injury indices shown in Fig. 9 indicating the simulations using vehicle contact characteristics from Mizuno and Liu have lowers errors, the Martinez and EU NCAP simulations rank 2nd and 3rd respectively. Accordingly, future work must focus on amendments to the MADYMO pedestrian model and try to reconstruct the kinematic and injury response of the pedestrian in each test precisely to improve its predictive capacity for ground contact, and on assessing the predictive capacity of other multibody and finite element model formulations (Maeno and Hasegawa, 2001; Iwamoto et al., 2003; Untaroiu et al., 2016). This is needed before a model can be confidently applied to assess ground contact injury countermeasures (either by new technology or by vehicle front shape changes). Similarly, it is clear that the MADYMO pedestrian model currently has limited potential for application to individual collision reconstruction purposes, though there have been substantial applications of this in the literature (Shen and Jin, 2008).

6. Limitations

There are several limitations to this study. Firstly, the experimental data is based on cadaver testing and it is understood that a living human response would be different, especially for the two 20kph tests where voluntary motion and muscle contraction are likely to play significant roles. Although the majority of pedestrians are largely struck from the side by the front of vehicles, real-world collisions are of course variable, and the available experiments do not provide a means to assess the predictive capacity of the model for other impact angles. Only one pedestrian model formulation was assessed, and it is possible that a different multibody or a finite element model would perform better. The models were globally scaled based on height and mass, not as an individual body segment level. The experimental measurements of the pre-impact joint angles of the cadavers were not precisely known.

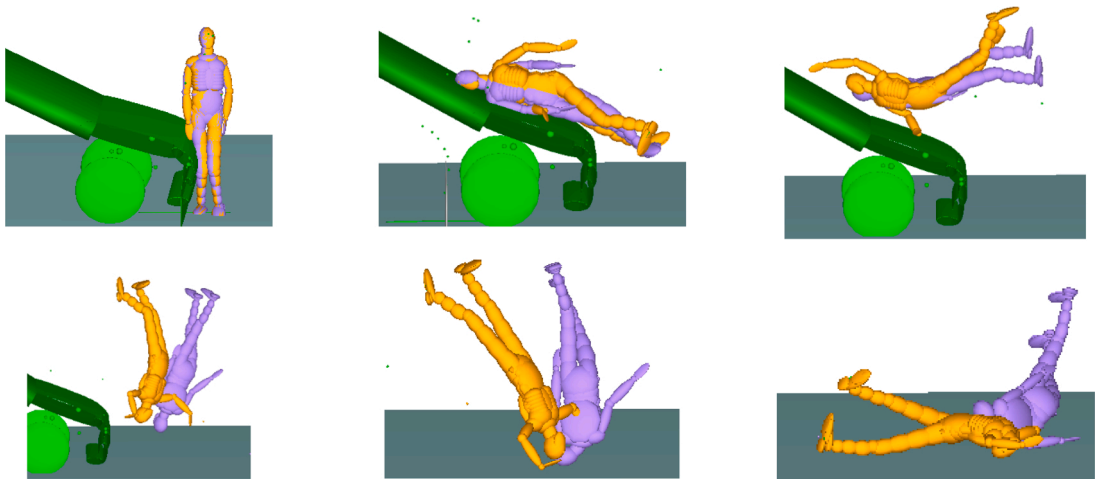

Fig. 13. Sequence of baseline pedestrian model (orange) and the model with added damping kinematics (purple) in vehicle crash for Test 01.

7. Conclusions

We have presented the first assessment of a computational model (here the MADYMO ellipsoid multibody pedestrian model) for predicting pedestrian flight and ground contact following a vehicle collision. A comparison with six cadaver tests performed over the speed range 20–30kph and with three different vehicle types and pedestrian sizes showed good capacity to predict vehicle contact times, but differences between the models and experiments manifested prior to vehicle pedestrian separation, and resulted in considerable differences in the ground contact kinematics. The resulting head injury predictions based on the ground contact *HIC* and *BrIC* scores showed limited capacity of the model to replicate individual experiments. Sensitivity studies showed substantial influences of the vehicle- pedestrian contact characteristic and some of the initial pedestrian joint angles on the subsequent ground contact injury predictions. Further work is needed to improve the predictive capacity of the MADYMO pedestrian model for ground contact injury predictions.

Author statement

Ciaran Simms is pleased to submit this revised paper on behalf of all authors.

Declaration of Competing Interest

The authors have no known conflicts of interest in relation to publication of this paper.

Acknowledgement

The authors would like to thank EURONCAP for generous provision of the impactor data. The support of the China Scholarship Council (CSC) is highly appreciated.

Appendix A. Information of vehicle and pedestrian cadavers tested in (Shang et al., 2020)

Table A1

Table A1
Summary of tests performed in (Shang et al., 2020).

Test number	Vehicle model	Vehicle speed (km/h)	Pedestrian age (y/o)	Pedestrian sex	Pedestrian height (m)	Pedestrian mass (kg)	NBLEH[c]
Test 01	Peugeot 307	30.5	88	Male	1.74	66	0.7
Test 02	Peugeot 307	30.4	83	Male	1.72	69	0.7
Test 03	Citroen C4	20.4	94	Male	1.67	64	0.9
Test 04	Citroen C4	21.0	83	Male	1.67	55	0.9
Test 05	Renault Kangoo II	30.1	94	Female	1.58	38	1.2
Test 06	Renault Kangoo II	30.4	86	Male	1.62	69	1.1

[c] NBLEH: Normalised bonnet leading edge height (Vehicle bonnet leading edge height/ pedestrian hip height).

Appendix B. Steps of defining and validating the movement input of the MB vehicle models

(1) According to the width of the vehicle and the markers on the lab ground, using ginput function in Matlab to pick 2 pairs of points (a1 and a2, a3 and a4) which define 1 m in y = 0 and y = 0.75, then the scale (the length of b1b2, the coordinates of b1 and b2 are in line with the coordinates of the reference points picked from the side of the vehicle) can be calculated based on the mathematical relation, see Fig. B1 (a). The scale in Y direction depends on the coordinates of the points P1 and P2 in Fig. B1 (b).
(2) P1 is a reference point which can be used to find the tracking point P0 based on their relative positional relationship. Pick two points P1 and P2 in a line on the side of the vehicle, then the angular change of the vehicle can be calculated.

After the X and Z motion of the tracking point and the angle of the vehicle were calculated, the polynomial fittings (third-degree polynomial for X motion, ninth-degree polynomial for Z motion, fourth-degree polynomial for vehicle angle. Different orders were used for

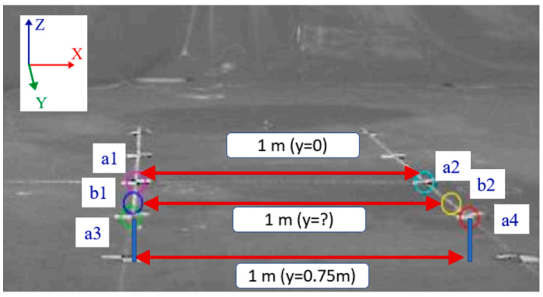

(a) Demonstration of choosing the scale

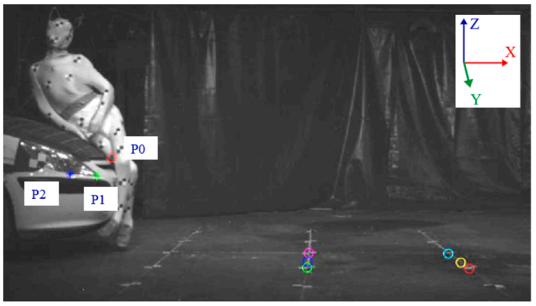

(b) Demonstration of choosing the tracking point P0

Fig. B1. The steps of choosing the tracking point.

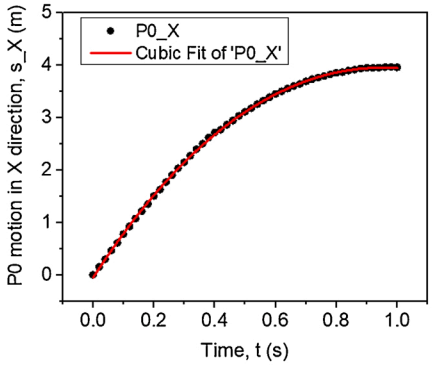

(a) Vehicle X motion

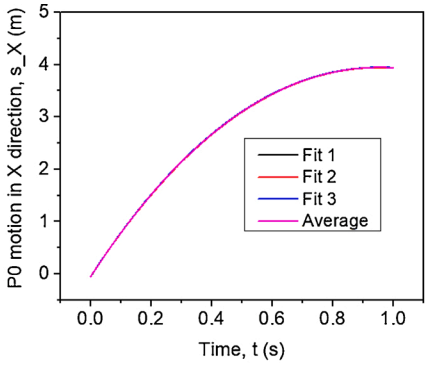

(b) 3 fitting curves of P0 X motion as well as the average curve

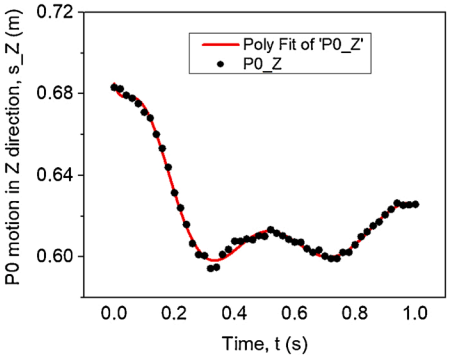

(c) Vehicle Z motion

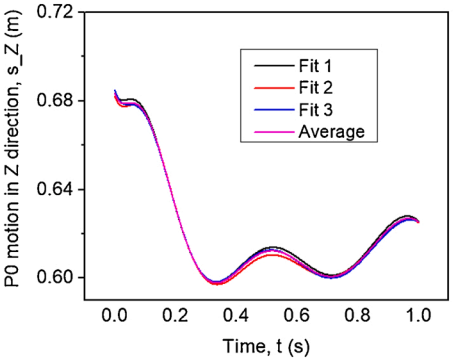

(d) 3 fitting curves of P0 Z motion as well as the average curve

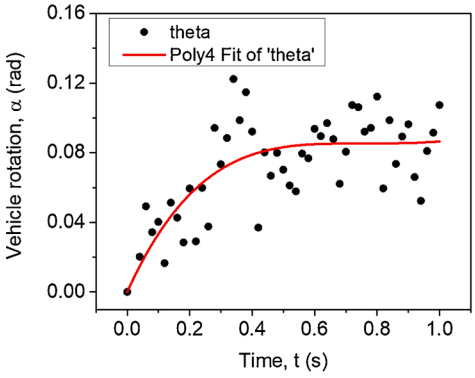

(e) Vehicle angle

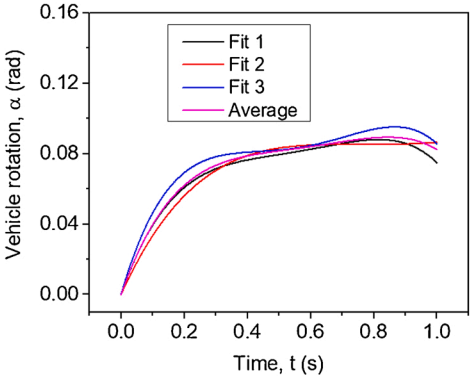

(f) 3 fitting curves of vehicle angle as well as the average curve

Fig. B2. The fitting curves of the motion of the tracking point.

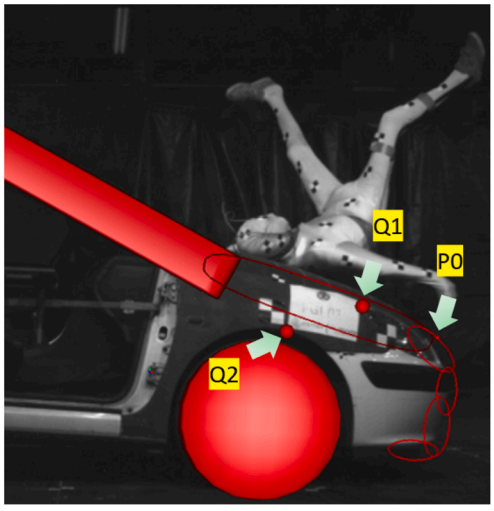

(a) The locations of two checking points

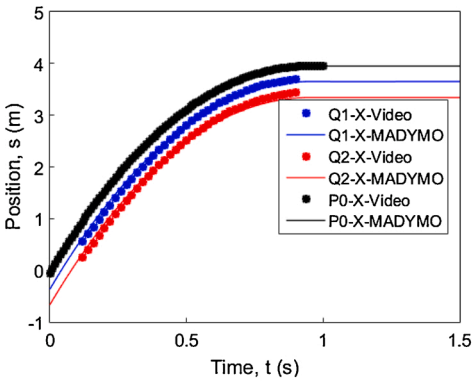

(b) X motion

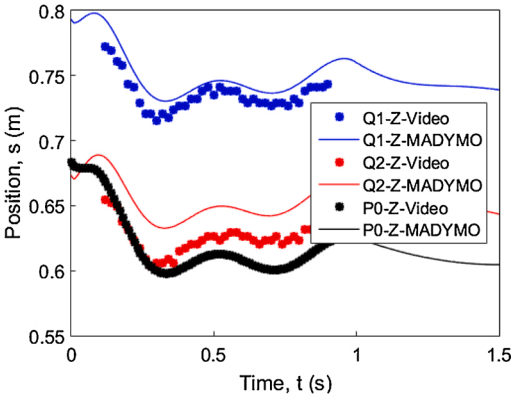

(c) Z motion

Fig. B3. The comparison of input and output motions of checking points.

respective best matching of the fitting curve) were applied to fit the time history curves to ensure a smooth MB vehicle movement. Take Test 01 for instance, the motion of the tracking points corresponding the fitting curves are shown in Fig. B2 (a), (c) and (e). It should be noted since the changes in the Z direction and theta (vehicle angle) are very small, a minor difference can result in relatively big errors when tracking the points P1 and P2. To reduce the error, the movements were tracked three times and averaged for each test, see Fig. B2 (b), (d) and (f).

The input and output motions of the tracking point P0, as well as two other checking points Q1 and Q2 [as demonstrated in Fig. B3 (a)], were compared to check whether the MB vehicle model moves as well as the input motions. Fig. B3 (b) and (c) show that the movement of the tracking point P0 and the input is identical. For the two other reference points, the horizontal motion obtained from the video of the test and motion obtained from the MADYMO simulation output is closely related. The differences in vertical direction were small (up to 3 cm) and may be due to the vehicle's rotation angle, which can be ignored. The checking point results indicate the feasibility of using the tracking system to capture the vehicle movement.

Fig. C1. Test 01: Sequences of vehicle-pedestrian impact experiment compared with MB simulations. Contact characteristic of vehicle front applied from (Green model: EU NCAP; Blue model: Martinez; Red model: Mizuno). Test 02: Sequences of vehicle-pedestrian impact experiment compared with MB simulations. Contact characteristic of vehicle front applied from (Green model: EU NCAP; Blue model: Martinez; Red model: Mizuno). Test 03: Sequences of vehicle-pedestrian impact experiment compared with MB simulations. Contact characteristic of vehicle front applied from (Green model: EU NCAP; Blue model: Martinez; Red model: Mizuno). Test 04: Sequences of vehicle-pedestrian impact experiment compared with MB simulations. Contact characteristic of vehicle front applied from (Green model: EU NCAP; Blue model: Martinez; Red model: Mizuno). Test 05: Sequences of vehicle-pedestrian impact experiment compared with MB simulations. Contact characteristic of vehicle front applied from (Green model: EU NCAP; Blue model: Martinez; Red model: Mizuno). Test 06: Sequences of vehicle-pedestrian impact experiment compared with MB simulations. Contact characteristic of vehicle front applied from (Green model: EU NCAP; Blue model: Martinez; Red model: Mizuno).

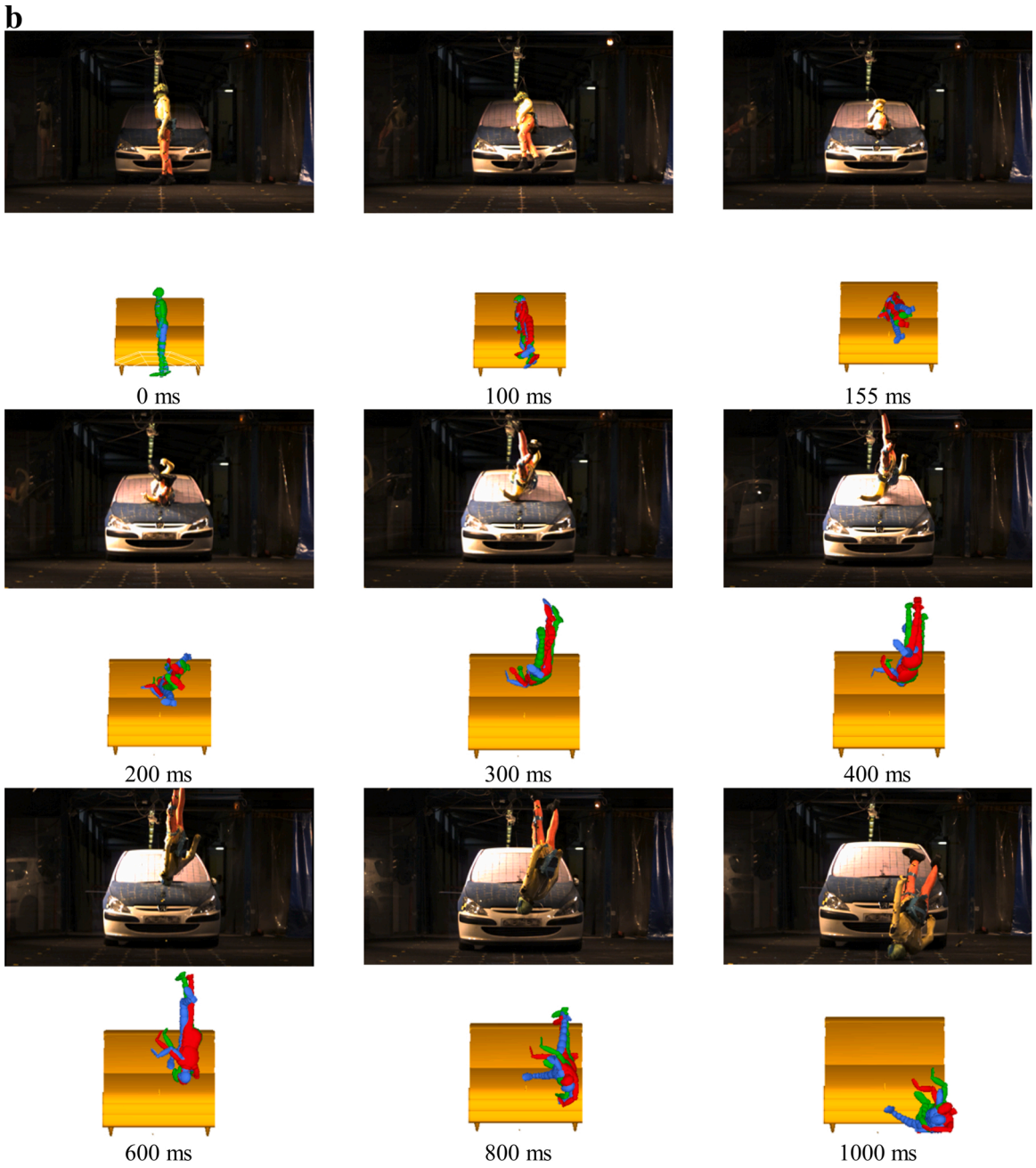

Fig. C1. (*continued*).

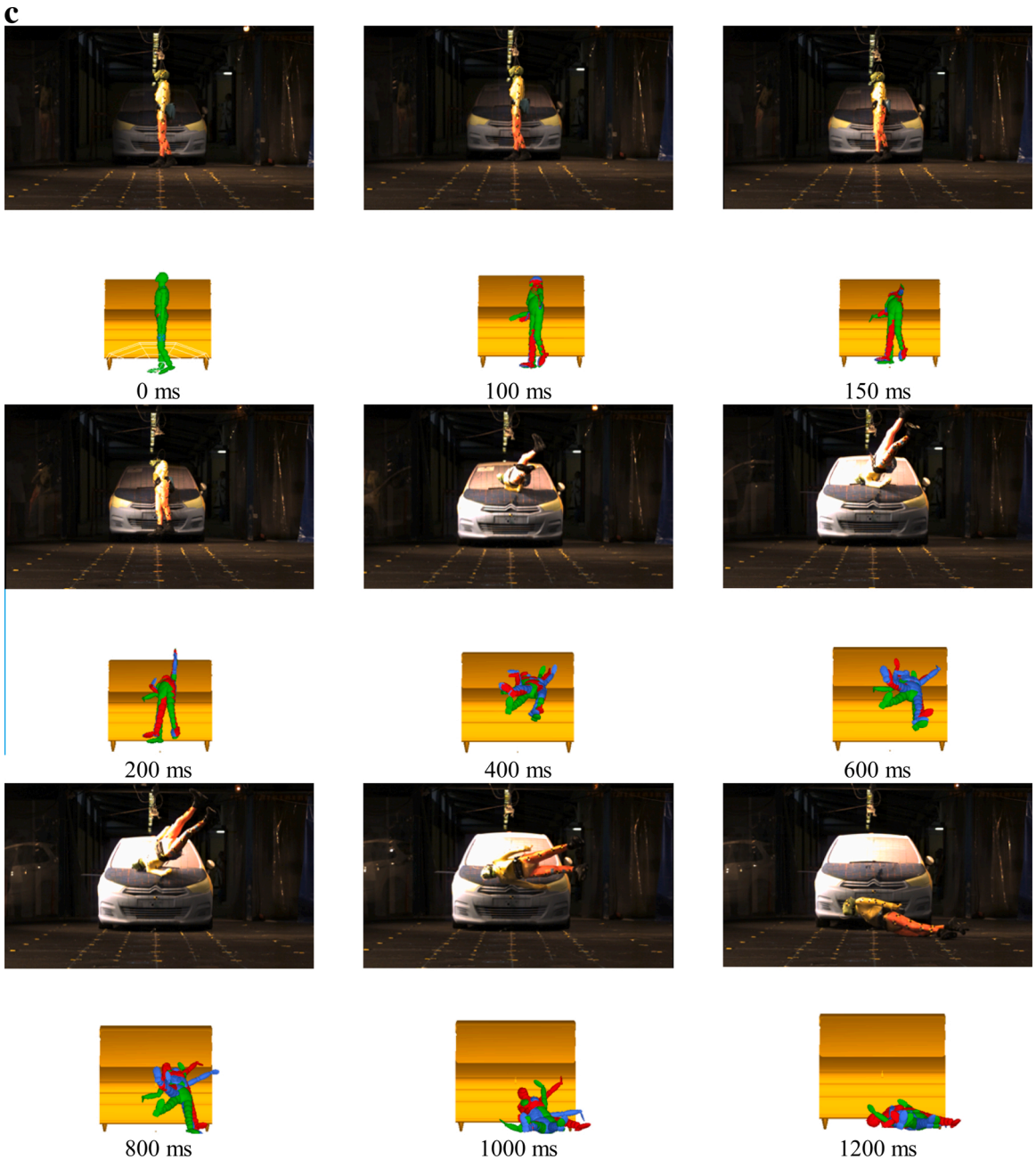

Fig. C1. (*continued*).

Fig. C1. (*continued*).

Fig. C1. (*continued*).

Appendix C. Sequences of vehicle-pedestrian impact experiment compared with MB simulations in front view

Fig. C1. (*continued*).

References

Barry, F., Simms, C., 2016. Assessment of head-ground impact patterns in real world pedestrian-vehicle collisions. Proceedings of the IRCOBI Conference Proceedings.
Coley, G., De Lange, R., De Oliveira, P., Neal-Sturgess, C.E., Happee, R., 2001. Pedestrian human body validation using detailed real-world accidents. Proceedings of the Proceedings of the IRCOBI Conference.
Crocetta, G., Piantini, S., Pierini, M., Simms, C., 2015. The influence of vehicle front-end design on pedestrian ground impact. Accid. Anal. Prev. 79, 56–69.
Delange, R., Vanrooij, L., Happee, R., Liu, X., 2006. Validation of Human Pedestrian Models Using Laboratory Data As Well As Accident Reconstruction.
Elliott, J., Simms, C., Wood, D., 2012. Pedestrian head translation, rotation and impact velocity: the influence of vehicle speed, pedestrian speed and pedestrian gait. Accid. Anal. Prev. 45, 342–353.
Euro-Ncap, 2010. Pedestrian Testing Protocol.
https://www.euroncap.comEuro-Ncap, .
Gabler, L.F., Crandall, J.R., Panzer, M.B., 2018. Development of a metric for predicting brain strain responses using head kinematics. Ann. Biomed. Eng. 46 (7), 972–985.
Han, Y., Li, Q., Wang, F., Wang, B., Mizuno, K., Zhou, Q., 2018. Analysis of pedestrian kinematics and ground impact in traffic accidents using video records. Int. J. Crashworthiness 1–10.

Hobbs, C.A., Mcdonough, P.J., 1998. Development of the european new car assessment programme (euro ncap). Regulation 44, 3.
Ishikawa, H., Kajzer, J., Schroeder, G., 1993. Computer simulation of impact response of the human body in car-pedestrian accidents. SAE Technical Paper.
Iwamoto, M., Omori, K., Kimpara, H., Nakahira, Y., Tamura, A., Watanabe, I., Miki, K., Hasegawa, J., Oshita, F., Nagakute, A., 2003. Recent advances in thums: development of individual internal organs, brain, small female and pedestrian model. Proceedings of the Proceedings of 4th European LS Dyna Users Conference 1–10.
Kajzer, J., Cavallero, C., Bonnoit, J., Morjane, A., Ghanouchi, S., 1993. Response of the knee joint in lateral impact: effect of bending moment. Proceedings of the Proceedings of the IRCOBI Conference 105–116.
Kerrigan, J.R., Crandall, J.R., Deng, B., 2007. Pedestrian kinematic response to mid-sized vehicle impact. Int. J. Veh. Saf. 2 (3), 221–240.
Khaykin, A., Larner, D.L., 2016. Adhesive Vehicle Front End for Mitigation of Secondary Pedestrian Impact. Google Patents.
Li, G., Yang, J., Simms, C., 2016. A virtual test system representing the distribution of pedestrian impact configurations for future vehicle front-end optimization. Traffic Inj. Prev. 17 (5), 515–523.
Li, G., Wang, F., Otte, D., Cai, Z., Simms, C., 2018. Have pedestrian subsystem tests improved passenger car front shape? Accid. Anal. Prev. 115, 143–150.
Liu, X.J., Yang, J.K., Lövsund, P., 2002. A study of influences of vehicle speed and front structure on pedestrian impact responses using mathematical models. Traffic Inj. Prev. 3 (1), 31–42.
Maeno, T., Hasegawa, J., 2001. Development of a finite element model of the total human model for safety (thums) and application to car-pedestrian impacts. SAE Technical Paper.
Martinez, L., Guerra, L.J., Ferichola, G., Garcia, A., Yang, J., 2007. Stiffness corridors of the european fleet for pedestrian simulations. Proceedings of the 20th International Technical Conference on the Enhanced Safety of Vehicles (ESV) National Highway Traffic Safety Administration.
Mizuno, K., Kajzer, J., 2000. Head injuries in vehicle-pedestrian impact. SAE Technical Paper.
Serre, T., Masson, C., Perrin, C., Chalandon, S., Llari, M., Cavallero, C., Py, M., Cesari, D., 2006. Pedestrian and cyclist accidents: a comparative study using in-depth investigation, multibody simulation and experimental test. Proceedings of the IRCOBI Conference.
Shang, S., 2020. Pedestrian Whole Body Ground Contact Mechanisms and Head Injury Assessment Following Vehicle Impact. Trinity College Dublin.
Shang, S., Otte, D., Li, G., Simms, C., 2018. Detailed assessment of pedestrian ground contact injuries observed from in-depth accident data. Accid. Anal. Prev. 110, 9–17.
Shang, S., Masson, C., Teeling, D., Py, M., Ferrand, Q., Arnoux, P.-J., Simms, C., 2020. Kinematics and dynamics of pedestrian head ground contact: a cadaver study. Saf. Sci. 127, 104684.
Shen, J., Jin, X., 2008. Improvement in numerical reconstruction for vehicle—pedestrian accidents. Proc. Inst. Mech. Eng. Part D: J. Automobile Eng. 25–39.
Shi, L., Han, Y., Huang, H., He, W., Wang, F., Wang, B., 2019. Effects of vehicle front-end safety countermeasures on pedestrian head injury risk during ground impact. Proc. Inst. Mech. Eng. Part D: J. Automobile Eng. 0954407019828845.
Simms, C.K., Wood, D.P., 2006. Effects of pre-impact pedestrian position and motion on kinematics and injuries from vehicle and ground contact. Int. J. Crashworthiness 11 (4), 345–355.
Takhounts, E.G., Craig, M.J., Moorhouse, K., Mcfadden, J., Hasija, V., 2013. Development of brain injury criteria (bric). SAE Technical Paper.
The-Blueprints, http://www.the-blueprints.com/.
Triana, C., Fajardo, F., 2013. Experimental study of simple harmonic motion of a spring-mass system as a function of spring diameter. Rev. Bras. Ensino Fã-sica 35 (4), 1–8.
Untaroiu, C.D., Meissner, M.U., Crandall, J.R., Takahashi, Y., Okamoto, M., Ito, O., 2009. Crash reconstruction of pedestrian accidents using optimization techniques. Int. J. Impact Eng. 36 (2), 210–219.
Untaroiu, C.D., Putnam, J.B., Schap, J., Davis, M.L., Gayzik, F.S., 2016. Development and preliminary validation of a 50th percentile pedestrian finite element model. Proceedings of the ASME 2015 International Design Engineering Technical Conferences and Computers and Information in Engineering Conference.
Van Hoof, J., De Lange, R., Wismans, J.S., 2003. Improving pedestrian safety using numerical human models. SAE Technical Paper.
Van Rooij, L., Bhalla, K., Meissner, M., Ivarsson, J., Crandall, J., Longhitano, D., Takahashi, Y., Dokko, Y., Kikuchi, Y., 2003. Pedestrian crash reconstruction using multi-body modeling with geometrically detailed, validated vehicle models and advanced pedestrian injury criteria. Proceedings of the 18th ESV Conference.
Who, 2018. Global Status Report on Road Safety 2018. World Health Organization.
Who, https://extranet.who.int/roadsafety/death-on-the-roads/#ticker.
Xu, J., Shang, S., Yu, G., Qi, H., Wang, Y., Xu, S., 2016. Are electric self-balancing scooters safe in vehicle crash accidents? Accid. Anal. Prev. 87, 102–116.
Yang, J., Lovsund, P., 1997. Development and validation of a human-body mathematical model for simulation of car-pedestrian collisions. In: Proceedings of the Proc. of the Int. IRCOBI Conf. Hanover (Germany), pp. 133–149.
Yang, J., Rzymkowski, C., Kajzer, J., 1993. Development and validation of a mathematical breakable leg model. Proceedings of the Proceedings of the International Research Council on the Biomechanics of Injury Conference 175–186.
Yang, J., Kajzer, J., Cavallero, C., Bonnoit, J., 1995. Computer simulation of shearing and bending response of the knee joint to a lateral impact. SAE Technical Paper.
Yao, J., Yang, J., Otte, D., 2008. Investigation of head injuries by reconstructions of real-world vehicle-versus-adult-pedestrian accidents. Saf. Sci. 46 (7), 1103–1114.
Zou, T., Shang, S., Simms, C., 2019. Potential benefits of controlled vehicle braking to reduce pedestrian ground contact injuries. Accid. Anal. Prev. 129, 94–107.